The Mechanical Modeling of Thermomechanical Processes for Thin-Walled Cylinders

Biljana Prochaska
University of Banja Luka
Faculty of Mechanical Engineering
Bosnia and Herzegovina

Nebojša Radić
Full professor
University of East Sarajevo
Faculty of Mechanical Engineering
Bosnia and Herzegovina

Srđan Bulatović
Institute for Testing of Materials
(IMS Institute)
Bulevar vojvode Mišića 43, Belgrade
Serbia

The problem of stress in perforated thin-walled cylinders due to mechanical and thermal load was analyzed for cases where the load of the system varies both along the cylinder circumference and axially. Starting from the solution and considerations for a smooth thin-walled cylinder, the concept was expanded and the distribution of deformations caused by thermal loads on the cylinder and the resulting stresses in the structure of the thin-walled perforated cylinder was observed for a specific form of perforation.
The cylindrical perforated burner is one of the main elements of premixed condensing boiler for home heating systems. The quality of combustion, and thus the heat load on the outer sheath of the burner, largely depends on the layout, shape and dimensions of the perforation.
This paper presents the mechanical modeling of thermomechanical processes of a cylindrical gas burner with premixing for a triangular layout or the so-called checkerboard shape of perforation.

Keywords: *thin-walled cylinder, deformations and stresses of thin-walled cylinders, thermomechanical modeling, thermal stress, premixed cylindrical burner, perforation*

1. INTRODUCTION

The center of research in this paper is the problem of stress in perforated thin-walled cylinders due to mecha–nical and thermal loads for cases where the system load varies. This problem was observed in premixed conden–sing gas burners for domestic heating systems, Figure 1.

Nowadays the industry focuses on reducing the emission of harmful combustion. Development of devi–ces and technologies follows this globally set goal. A premixed condensing gas burner is one such device.

One of the most important components of this device is certainly a cylindrical perforated gas burner located in the heat exchanger. A number of properties of the whole device depend on the design of this burner.

The basic characteristics of these new flexible bur–ners with premixing, more precisely atmospheric pre–mixed metal burners, are that they are made without water cooling and have a great ability to modulate po–wer 1:3, and even more. They achieve a reduced emi–ssion of harmful combustion products that does not ex–ceed 50 [mg/kWh].Greater flexibility also applies to different gaseous fuels used for the same device. This usually depends on the place where the device is used, whether local natural gas, liquefied petroleum gas, bio–gas and the like are used. As such, the construction of the device itself is subject to research from various aspects.

Perforated burners made of thin steel material are thermally and mechanically very durable, and at the same time their price is competitive.They should be carefully designed to form a front of stable thin flames, on which low emissions of CO and NOx harmful com–bustion products depend.Due to the required flexibility, flame fluctuations often occur in the operation of the burner, which then creates an uneven heat load. The design of the burner should ensure the minimum heat load generated during the combustion of different types of gas on the burner body at different operating modes.

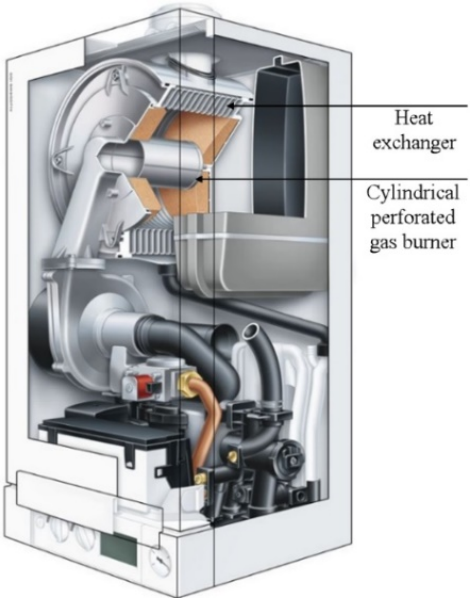

Figure 1. A condensing gas burner with premixing for domestic heating systems, (https://viessmanndirect.co.uk/Catalogue/Commercial-Gas-Boilers, 2022)

The geometry of a repeated geometric perforation pattern on the cylinder of a gas burner (Figure 2, Figure 3) plays one of the key roles in creating the heat load.

Received: April 2024, Accepted: June 2024
Correspondence to: Biljana Prochaska, PhD
Faculty of Mechanical Engineering Banja Luka,
Stepe Stepanovića 71, 78000 Banja Luka, BiH
E-mail: biljana.prochaska@mf.unibl.org
doi: 10.5937/fme2403429P

The process of the burner's operation takes place in such a way that the gas comes from inside the burner, the inner cylindrical sheath distributes it evenly and passes it towards the next surface, i.e. the outer cylin–drical sheath. The gas then flows through small ope–nings in the outer sheath. Here, on the surface of the outer sheath, ignition occurs, when a uniform flame is formed. The flame is formed on the entire cylindrical surface of the outer sheath.

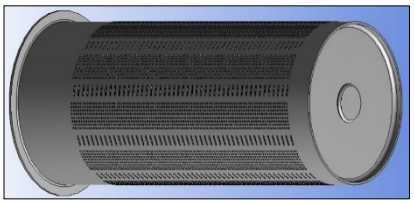

Figure 2. A 3D model of a cylindrical perforated gas burner showing a demanding outer

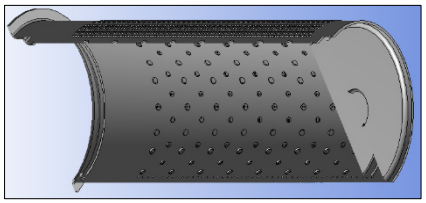

Fifure 3. Cross-section of the body of the gas burner, where the inner sheath is also visible

2. RESEARCH REVIEW

The improvement of gas condensing boilers with pre–mixing has been the focus of many researchers. Imp–roving individual parts of the construction of these boilers has been investigated from different aspects. Thus, some authors dealt with NOx formation in reali–stic, axi-symmetric condensing boiler setups featuring lean combustion of methane stabilized by a porous cylindrical burner using a dedicated numerical model [1].Some pointed to problems in the variation of gas quality [2]. In paper [3], performed 3-dimensional numerical simulations with skeletal kinetic mechanisms are performed to determine the structure of premixed methane-air flames issuing from two-slits patterns. Others dealing with construction elements [4] focus in the same direction.This paper analyses the outer cy–linder of the premixed burner in relation to thermal stress. Numerical finite element method (FEM) analysis was performed based on experimental measurements and computational fluid dynamics (CFD) input data. Similarly, in their paper [5] the authors focused on the investigation of geometric parameters of a flat per–forated burner. In [6,7], they optimized and verify the proposed geometric changes of the burner with the help of CFD numerical simulation. In the paper [8], the authors analyzed the repeated pattern in the perforation of a plate burner for different layouts of openings, triangular and linear. Other authors [9] describes steps in development of the cylindrical premixed burner taken in order to fulfil market requests as well as environmental standards, taking in to consideration that fuels which can be used, can have different quality levels. An analytical solution to stresses and displacements in a long functionally graded hollow cylinder subjected to uniform heat generation and internal pressure was given by the authors in [10]. Stress analysis showed that the stresses in the cylinder decrease significantly for a certain interval of material parameters.In the paper [11], the authors usedthe CFD analysis to improve geomet–rical parameters of the basic model of a supersonic ejector and optimized its operation in different operating conditions. The problem of thermal variable stress in thick hollow cylinders was dealt with in [12]. The inf–luence of the temperature gradient on the bending of thin plates was dealt with in [13]. Those authors deter–mined, in a closed analytical form, deflection of a thin plate that causes a constant temperature gradient. They showed that the deflection did not depend on the thic–kness of the plate, but on its dimension in the middle plane. In their work [14], the authors derived an analy–tical solution for radial, tangential and axial thermal stress in a hollow cylinder with uniform internal gene–rated heat for thermal boundary conditions of convec–tive heating on the inner surface of the cylinder and convective cooling on the outer surface of the cylinder. In the paper [15], thin-walled plates and tubes were experimentally investigated to quantify the effects of thermal loads on the through-thickness temperature gra–dients. In [16] the circumferential stress around a triangular or square opening in a finite isotropic plane was studied under thermal loads. Paper [17] presents the solution for the thermal stress of the double Fourier series. This is based on the Sanders linear shell theory with additional heat load terms.

In the available literature, it has not been noticed that someone has created a comprehensive unique mo–del that would unify all the influence segments and in such a way optimize the geometry of the cylindrical burner.

3. THE MATHEMATICAL MODEL FOR A THIN-WALLED CYLINDER WITH UNEVEN HEAT LOAD

The problem of stress in thin-walled cylinders due to mechanical and thermal load was analyzed for cases where the load of the system varies along the circum–ference of the cylinder and axially.

In the first part of the analysis, the behavior of a smooth thin-walled cylinder was observed, while the second part of the analysis also included a thin-walled cylinder with perforation.

3.1. The mathematical model for a thin-walled smooth cylinder with uneven heat loads

The Sanders stress model for a thin-walled cylinder under the influence of deformations was chosen [18].

First, the distribution of deformations caused by the thermal load on the cylinder and the resulting stresses in the structure of the cylinder, i.e. the sheath burner, which were subsequently developed by Tot [17] and Wilson [19], were observed.

The search for the solution of the system of diffe–rential equations for deformations and stresses via the double Fourier series was applied.

The temperature field is the only load acting on the cylindrical perforated burner exposed to high tempe–ratures on the surface of the outer sheath. For this reason, a suitable analytical function $T(z,\phi)$ of the tem–perature distribution of the external action on the sur–face of the sheath was chosen, [19]. A simple function consisting of segments of analytical smooth functions by defined areas was chosen. This analytical function is specially developed into a double Fourier series in order to obtain the temperature coefficients $T_{n,m}$ that figure in the solutions of the system of differential equations for deformations and stresses.

3.2. The relationship between stress and strain

The basic deformation equations for thin shells under the influence of stress and heat, neglecting radial defor–mations and stresses, are given by the expressions:

$$\begin{aligned} e_z &= \frac{\sigma_z}{E} - \nu\frac{\sigma_\phi}{E} + \alpha T \\ e_\phi &= \frac{\sigma_\phi}{E} - \nu\frac{\sigma_z}{E} + \alpha T \\ e_{z\phi} &= \frac{\tau_{z\phi}}{G} \end{aligned} \tag{1}$$

Here αT is the thermal deformation. The total de–formations at an arbitrary point $r$are given by the com–ponents:

$$\begin{aligned} e_z &= \varepsilon_z + rk_z \\ e_\phi &= \varepsilon_\phi + rk_\phi \\ e_{z\phi} &= \varepsilon_{z\phi} + rk_{z\phi} \end{aligned} \tag{2}$$

It follows that the stress equations are:

$$\begin{aligned} \sigma_z &= \frac{E}{1-\nu^2}(\varepsilon_z + \nu\varepsilon_\phi) + \frac{Er}{1-\nu^2}(k_z + \nu k_\phi) - \frac{E\alpha T}{1-\nu} \\ \sigma_\phi &= \frac{E}{1-\nu^2}(\varepsilon_\phi + \nu\varepsilon_z) + \frac{Er}{1-\nu^2}(k_\phi + \nu k_z) - \frac{E\alpha T}{1-\nu} \\ \tau_{z\phi} &= \frac{E}{2(1+\nu)}(\varepsilon_{z\phi} + rk_{z\phi}) \end{aligned} \tag{3}$$

3.3. The relationship between deformations and displacements

Figure 4 shows the directions of the cylindrical coor–dinate system, displacements, and resultants of forces and moments.

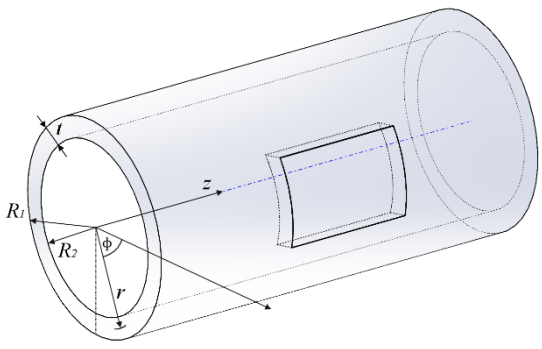

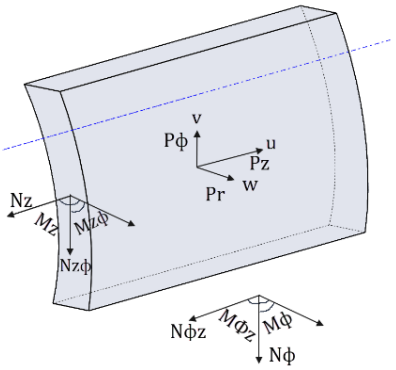

Figure 4. Components of the shell in the cylindrical coor–dinate system

Now the equations of deformation depending on the displacement given by the shell components in the cylindrical system are $u(z,\phi)$, $v(z,\phi)$, $w(z,\phi)$ given in the given order. Rrepresents the radius of the central surface of the shell.

$$\begin{aligned} \varepsilon_z &= \frac{\partial}{\partial z}u(z,\phi), \\ \varepsilon_\phi &= \frac{\frac{\partial}{\partial\phi}v(z,\phi) + w(z,\phi)}{R}, \\ \varepsilon_{z\phi} &= \frac{1}{2}\left(\frac{\partial}{\partial z}v(z,\phi) + \frac{1}{R}\frac{\partial}{\partial\phi}u(z,\phi)\right), \\ k_z &= -\frac{\partial^2}{\partial z^2}w(z,\phi), \\ k_\phi &= -\frac{\frac{\partial^2}{\partial\phi^2}w(z,\phi) - \frac{\partial}{\partial\phi}v(z,\phi)}{R^2}, \\ k_{z\phi} &= -\frac{1}{R}\frac{\partial^2}{\partial\phi\partial z}w(z,\phi) + \frac{3}{4R}\frac{\partial}{\partial z}v(z,\phi) - \\ &\quad -\frac{1}{4R^2}\frac{\partial}{\partial\phi}u(z,\phi) \end{aligned} \tag{4}$$

The resultants of the forces and moments of the forces were obtained by integration over the thickness of the shell t, i.e. sheath, using the Sanders' definition:

$$\begin{aligned} N_z &= \int_{-t/2}^{t/2}\sigma_z dr, & M_z &= \int_{-t/2}^{t/2}\sigma_z r dr, \\ N_\phi &= \int_{-t/2}^{t/2}\sigma_\phi dr, & M_\phi &= \int_{-t/2}^{t/2}\sigma_\phi r dr, \\ N_{z\phi} &= \int_{-t/2}^{t/2}\tau_{z\phi} dr, & M_{z\phi} &= \int_{-t/2}^{t/2}\tau_{z\phi} r dr \end{aligned} \tag{5}$$

Substituting (3) into (5) and after carrying out the integration, the following can be written:

$$\begin{aligned} N_z &= K\left(\varepsilon_z + \nu\varepsilon_\phi\right) - \frac{N_T}{1-\nu}, \\ N_\phi &= K\left(\varepsilon_\phi + \nu\varepsilon_z\right) - \frac{N_T}{1-\nu}, \end{aligned}$$

$$N_{z\phi} = Gt\varepsilon_{z\phi},$$
$$M_z = D\left(k_z + \nu k_\phi\right) - \frac{M_T}{1-\nu},$$
$$M_\phi = D\left(k_\phi + \nu k_z\right) - \frac{M_T}{1-\nu}, \quad (6)$$
$$M_{z\phi} = \frac{Gt^3\tau_{z\phi}}{12}$$

The thermal force and moment are introduced in the same way:

$$N_T = E\alpha \int_{-t/2}^{t/2} Tdr, \qquad M_T = E\alpha \int_{-t/2}^{t/2} Trdr \quad (7)$$

3.4. Applied heat loads

The temperature distribution changes almost linearly across the shell thickness *t*, Figure 4. Considering this, it is possible to express any temperature *T* at any point (*r, ϕ z*) by the thickness of the shell *t*, in the sense where T_M is the temperature in the middle of the shell, and T_D is the temperature difference between the upper and lower surfaces of the shell.Then the temperature at some point of the shell is:

$$T = T_M - \frac{T_D}{t} r \quad (8)$$

The result of integration is:

$$N_T = E\alpha \int_{-t/2}^{t/2} Tdr = E\alpha t T_M,$$
$$M_T = E\alpha \int_{-t/2}^{t/2} Trdr = \frac{-E\alpha t^2 T_D}{12} \quad (9)$$

Inserting (4) into (6) and by inserting expression (9), the values for the force resultants are obtained:

$$N_z = K\left(\frac{\nu\left(\frac{\partial}{\partial\phi}v(z,\phi) + w(z,\phi)\right)}{R} + \frac{\partial}{\partial z}u(z,\phi)\right) - K(1+\nu)\alpha T_M(z,\phi)$$
$$N_\phi = K\left(\nu\frac{\partial}{\partial z}u(z,\phi) + \frac{\frac{\partial}{\partial\phi}v(z,\phi) + w(z,\phi)}{R}\right) - K(1+\nu)\alpha T_M(z,\phi) \quad (10)$$
$$N_{z\phi} = \frac{1}{2}\,\frac{K(1-\nu)\left(R\frac{\partial}{\partial z}v(z,\phi) + \frac{\partial}{\partial\phi}u(z,\phi)\right)}{R}$$

and moments:

$$M_z = Kk\left(-\frac{\nu\left(\frac{\partial^2}{\partial\phi^2}w(z,\phi) - \frac{\partial}{\partial\phi}v(z,\phi)\right)}{R^2} + \frac{\partial^2}{\partial z^2}u(z,\phi)\right) + \frac{1}{12}K(1+\nu)\alpha t T_D(z,\phi)$$
$$M_\phi = Kk\left(\nu\frac{\partial^2}{\partial z^2}u(z,\phi) - \frac{\frac{\partial^2}{\partial\phi^2}w(z,\phi) - \frac{\partial}{\partial\phi}v(z,\phi)}{R^2}\right) + \frac{1}{12}K(1+\nu)\alpha t T_D(z,\phi) \quad (11)$$
$$M_{z\phi} = Kk(1-\nu)\left(-R\frac{\partial^2}{\partial\phi\partial z}w(z,\phi) + \frac{3}{4}R\frac{\partial}{\partial z}v(z,\phi) - \frac{1}{4}\frac{\partial}{\partial\phi}u(z,\phi)\right)$$

The Sanders stress model for a thin-walled cylinder reduces the general equilibrium equations to a system of three equations.External forces *Pi* are introduced into the system of equations (Figure 4), but in the final con–sideration and calculations they do not act because there are no external forces in the cylindrical burner model, so now the system of equations will have the following form:

$$Rd N_z + R\delta N_{z\phi} - \frac{1}{2}\delta M_{z\phi} = 0,$$
$$Rd N_{z\phi} + R\delta N_\phi + \frac{3}{2}d M_{z\phi} + \delta M_\phi = 0, \quad (12)$$
$$d^2 M_z + 2d\delta M_{z\phi} + \delta^2 M_\phi - RN_\phi = 0$$

Presentation of differential operators *d, δ* as $d = \frac{\partial}{\partial(z/R)} = R\frac{\partial}{\partial z}$, $\delta = \frac{\partial}{\partial\phi}$ gives a concise view of this system.

Explicit expressions for thermal forces and moments (10) and (11) are included in (12) three general equi–librium equations, which makes a system of three differential equations by *u*(*z, ϕ*), *v*(*z, ϕ*), *w*(*z, ϕ*).

After arranging these expressions, the matrix relation for the displacements associated with the loads is obtained.

The matrix form of the system of equilibrium differential equations is:

$$\begin{bmatrix} A_1 & B_1 & C_1 \\ A_2 & B_2 & C_2 \\ A_3 & B_3 & C_3 \end{bmatrix}\begin{bmatrix} u \\ v \\ w \end{bmatrix} = \begin{bmatrix} D_1 \\ D_2 \\ D_3 \end{bmatrix} \quad (13)$$

where A_i, B_i, C_i are differentiation operators, and ope–rators D_i refer to the thermal load.

After the action of the operator *d, δ* the equations of the system (12) are three linear differential equations.

A detailed description of the development of these equations is given in the doctoral dissertation [20].

By expressing the load and displacement compo–nents for the middle surface of the shell, the diameter *R,* linear differential equations can be solved in the form of a double Fourier series.

The choice of members of the development in the Fourier series implies simply supported boundary conditions at the ends of the cylinder. In the cross-sections located at the ends of the cylinder, it is allowed

to move the points in the axial direction, but their movement in the radial direction is prevented. A full discussion of boundary conditions in double Fourier series solutions is presented in paper [21]. The effect of the boundary conditions imposed by the Fourier series solution can be removed by considering the cylinder to be longer than its actual length.Limits on the axial expansion of the cylinder can be set. This allows displacements to be representedwith(14).

$$u(z,\phi)=\sum_{n=1}^{\infty}\left(\sum_{m=1}^{\infty}u_{n,m}\cos(n\phi)\cos\left(\frac{z\lambda_m}{R}\right)\right)$$
$$v(z,\phi)=\sum_{n=1}^{\infty}\left(\sum_{m=1}^{\infty}v_{n,m}\cos(n\phi)\cos\left(\frac{z\lambda_m}{R}\right)\right) \quad (14)$$
$$w(z,\phi)=\sum_{n=1}^{\infty}\left(\sum_{m=1}^{\infty}w_{n,m}\cos(n\phi)\cos\left(\frac{z\lambda_m}{R}\right)\right)$$

The temperature field is a suitable analytical func–tion $T(z,\phi)$ that can be represented by the(15):

$$T_M(z,\phi)=\frac{T_M}{4}\left\{1-\cos\frac{\pi\left[z-(l-b)\right]}{b}\right\}\left\{1-\cos\frac{\pi\left[\phi-(\pi-\theta)\right]}{\theta}\right\}$$
$$T_D(z,\phi)=\frac{T_D}{4}\left\{1-\cos\frac{\pi\left[z-(l-b)\right]}{b}\right\}\left\{1-\cos\frac{\pi\left[\phi-(\pi-\theta)\right]}{\theta}\right\} \quad (15)$$

Here it is $l-b\le z\le l+b$, $\pi-\theta\le\phi\le\pi+\theta$, and in other areas it is zero, where l, b and θ are the parameters that describe the position and width of the temperature distribution in axial and angular coordinates.

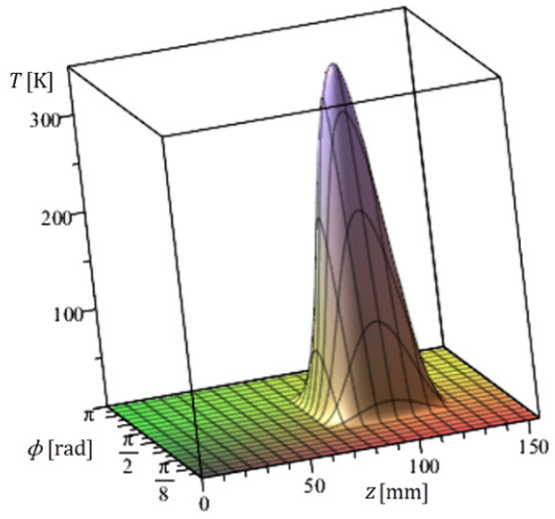

a)

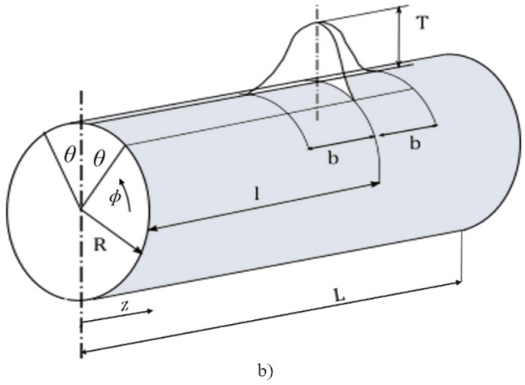

b)

Figure 5. Display of the given temperature distribution, a) in the orthogonal projection and b) display on the cylinder

Figure 5 presents a representation of the selected function of two variables that parametrically describes the temperature distribution in the limited area of the cylinder. It is suitable for double Fourier expansion. Figure 5 shows the function in the orthogonal projection in a) and the function on the cylinder, in b).

The function (15) was chosen to parametrically des–cribe the actual temperature field that appears on the cylinder as a load in the most realistic way. It consists of segments of analytical smooth functions in defined areas. Due to the axisymmetric nature of the cylinder, it is possible to arrange more such functions in order to obtain a more realistically described temperature field.

This function can certainly be developed as an analytical one into a special double Fourier series(16).

$$T_M(z,\phi)=\sum_{n=1}^{\infty}\left(\sum_{m=1}^{\infty}T_{M_{n,m}}\cos(n\phi)\sin\left(\frac{z\lambda_m}{R}\right)\right)$$
$$T_D(z,\phi)=\sum_{n=1}^{\infty}\left(\sum_{m=1}^{\infty}T_{D_{n,m}}\cos(n\phi)\sin\left(\frac{z\lambda_m}{R}\right)\right) \quad (16)$$

The obtained coefficients Tn,m of this order also ap–pear in the solutions of the system of differential equa–tions for deformations and stresses(12), that is, in the development of these equations into series.

It is now possible to solve the displacements $u(z,\phi)$, $v(z,\phi)$, $w(z,\phi)$ for the problem of a simply supported thin cylinder subjected to thermal loading.

When these equations are arranged, it is possible to express all forces and all moments via $u(z,\phi)$, $v(z,\phi)$, $w(z,\phi)$ and $T_M(z,\phi)$, $T_D(z,\phi)$.

By replacing the initial system of equations in the matrix form (13) with the Fourier expansion of indivi–dual terms (14) and (16), the following matrix equation is obtained:

$$\begin{bmatrix}A_1 & B_1 & C_1\\ A_2 & B_2 & C_2\\ A_3 & B_3 & C_3\end{bmatrix}\begin{bmatrix}\sum_{n=1}^{\infty}\left(\sum_{m=1}^{\infty}u_{n,m}\cos(n\phi)\cos\left(\frac{z\lambda_m}{R}\right)\right)\\ \sum_{n=1}^{\infty}\left(\sum_{m=1}^{\infty}v_{n,m}\cos(n\phi)\cos\left(\frac{z\lambda_m}{R}\right)\right)\\ \sum_{n=1}^{\infty}\left(\sum_{m=1}^{\infty}w_{n,m}\cos(n\phi)\cos\left(\frac{z\lambda_m}{R}\right)\right)\end{bmatrix}=\begin{bmatrix}\sum_{n=1}^{\infty}\left(\sum_{m=1}^{\infty}T_{n,m}\cos(n\phi)\sin\left(\frac{z\lambda_m}{R}\right)\right)\\ \sum_{n=1}^{\infty}\left(\sum_{m=1}^{\infty}T_{n,m}\cos(n\phi)\sin\left(\frac{z\lambda_m}{R}\right)\right)\\ \sum_{n=1}^{\infty}\left(\sum_{m=1}^{\infty}T_{n,m}\cos(n\phi)\sin\left(\frac{z\lambda_m}{R}\right)\right)\end{bmatrix} \quad (17)$$

After the action of the operators *Ai, Bi, Ci*on the sums of the members, the system of differential equa–tions turns into a system of algebraic equations.

All cosine and sine harmonics of different terms are linearly independent, so the original system is decom–posed into individual systems of three equations for *n,m*terms, where in each equation of the system the corresponding terms are associated with $u_{n,m}$, $v_{n,m}$, $w_{n,m}$.

A detailed description of the steps of determining the Fourier coefficients are given in the dissertation [20].

By solving this matrix equation, the solutions obtained for displacements are included in the expres–sions for forces (10) and moments (11), followed by:

$$
\begin{aligned}
N_z &= \frac{K}{R}\sum_n\sum_m\left[-\lambda_m w_{n,m} + \nu n u_{n,m} + \nu v_{n,m} - R(1+\nu)\alpha T_{M_{n,m}}\right]\cos n\phi \sin\left(\lambda_m \frac{z}{R}\right)\\
N_\phi &= \frac{K}{R}\sum_n\sum_m\left[n v_{n,m} + w_{n,m} - \nu\lambda_m u_{n,m} - R(1+\nu)\alpha T_{M_{n,m}}\right]\cos n\phi \sin\left(\lambda_m \frac{z}{R}\right)\\
N_{z\phi} &= \frac{K}{R}\sum_n\sum_m\left[\lambda_m v_{n,m} - n u_{n,m}\right]\sin n\phi \cos\left(\lambda_m \frac{z}{R}\right)\\
M_z &= \frac{D}{R^2}\sum_n\sum_m\left[(\lambda_m{}^2 + \nu n^2) w_{n,m} + \nu n v_{n,m} + \frac{R(1+\nu)\alpha t}{12k} T_{D_{n,m}}\right]\cos n\phi \sin\left(\lambda_m \frac{z}{R}\right)\\
M_\phi &= \frac{D}{R^2}\sum_n\sum_m\left[(\lambda_m{}^2 + \nu n^2) w_{n,m} + n v_{n,m} + \frac{R(1+\nu)\alpha t}{12k} T_{D_{n,m}}\right]\cos n\phi \sin\left(\lambda_m \frac{z}{R}\right)\\
M_{z\phi} &= \frac{D(1-\nu)}{R^2}\sum_n\sum_m\left(n\lambda_m w_{n,m} + \frac{3}{4}\lambda_m v_{n,m} + \frac{n}{4}u_{n,m}\right)\sin n\phi \cos\left(\lambda_m \frac{z}{R}\right)
\end{aligned}
\tag{18}
$$

Now the solutions for the stresses can be obtained:

$$
\begin{aligned}
\sigma_z &= \frac{N_z}{t} \mp \frac{6M_z}{t^2},\\
\sigma_\phi &= \frac{N_\phi}{t} \mp \frac{6M_\phi}{t^2},\\
\tau_{z\phi} &= \frac{N_{z\phi}}{t} \mp \frac{6M_{z\phi}}{t^2}.
\end{aligned}
\tag{19}
$$

3.5. The mathematical model for a thin-walled perforated cylinder

In relation to the papers mentioned, the concept was expanded here. Other authors considered stresses for a smooth thin-walled cylinder, while a perforated thin-walled cylinder was considered here.The model was extended to consider the stress of a perforated thin-walled cylinder subjected to an uneven temperature field. A triangular arrangement or the so-called checke–rboard shape of the perforation of the outer sheath was observed.

The geometric arrangement of repeated openings, holes and slits, the outer sheath, as well as their sizes, significantly affect the combustion process, fluid dyna–mics, and as a result, the thermal load on the structure.In order to introduce perforation elements into the analy–tical description of the temperature stress of the outer cylindrical sheath gas burner, a procedure for calcu–lating the equivalent elasticity parameters was intro–duced. The perforated plate is considered as a conti–nuous orthotropic plate that has three different moduli of elasticity E^*.

A starting assumption can be considered that the narrow strip part of the perforated rectangular plate is equivalent to the narrow strip part of the perforated cylinder whose curvature is neglected.

After obtaining the equivalent parameters of the modulus of elasticity E^*, Poisson's coefficient v^*, these parameters were introduced into the mathematical model of the smooth cylinder described in the previous section 3.1 and then the stresses for the perforated cylinder were calculated according to expression(19).

It is important to note that the analysis refers to the arrangement of only circular openings in the perfo–ration, without the part that has the shape of a slot. As is known, in addition to the circular shape of the opening, there is also the shape of the slit on the perforation of the real cylinder of the outer sheath burner, which must be takeninto account in subsequent research.

All parameters related to the equivalent flat plate in the cylinder model are tabular values of the properties of the material from which the cylinder is built, HAYNES 230.

Figure 6 shows a perforated plate having a perfo–ration pattern with a triangular arrangement of holes. The plate can be viewed as a series of longitudinal strips of width P in the observed plate, where$n$is the number of strips, Figure 7.

According to this pattern, also the width of the repe–ating basic motif is P. This width is the size from the center to the center of the weakening surface of the plate, i.e. hole, which can be seen in Figure 8.

The connection between the weakening surfaces, which remains a full part of the plate, is called the liga–ment h and its length represents the length of the liga–ment connection. η is defined as the efficiency of the connection, ligament of the non-perforated and perfo–rated plate. It represents a parameter for the calculation, the size of the weakening of the perforated surface of the plate com–pared to the non-perforated one.

It is defined as $\eta = \frac{h}{P}$. It served as an argument in the functional dependence that would show how much the observed parameters of the perforated surface wea–kened compared to the same parameters of the full sur–face without perforation.

For the overall behavior of the equivalent plate and the perforated plate to be the same, the deformations for the two plates should be equal.Based on [22]. the values of three different moduli of elasticity E^* of a continuous orthotropic plate were calculated as follows.

For the *x*- direction:

$$\frac{E_x^*}{E_x} = \frac{1}{f(\eta)} \tag{20}$$

where is:

$$f(\eta) = \frac{4}{\sqrt{3}}\left\{-\frac{\pi}{6} + \frac{2}{\sqrt{\eta(2-\eta)}} \arctan\left[\frac{(2-\eta)\tan\left(\frac{\pi}{12}\right)}{\sqrt{\eta(2-\eta)}}\right]\right\} + \frac{2\eta}{\sqrt{3}} - \frac{2\eta_{critical-x}}{\sqrt{3}} \tag{21}$$

This expression is correct for evaluating the efficiency of ligament connections, starting from the efficiency coefficient which is η = 100% up to the cri–tical efficiency coefficient of $\eta_{critical\text{-}x}$ = 100%. Here, 100% efficiency means that there are no holes on the plate, that is $h = P$, it follows that is $\eta = \frac{h}{P} = 1$, i.e. 100%, and an efficiency of 13.39% means that the holes start to overlap.

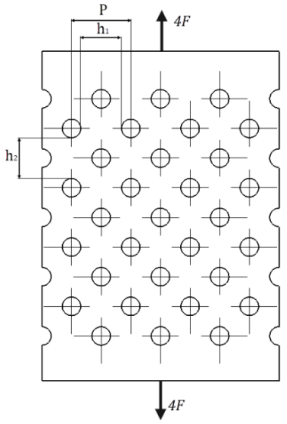

Figure 6. A sample of a loaded plate with a triangular arrangement of holes

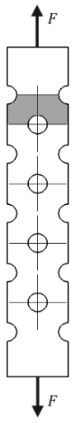

Figure 7. A separated strip from the sample with a triangular arrangement of openings

For the *y*-direction:

$$\frac{E_y^*}{E_y} = \frac{1}{g(\eta)} \tag{22}$$

$$g(\eta) = 2\sqrt{3}\left\{-\theta + \frac{2}{\sqrt{1-\frac{1}{\sqrt{3}}(1-\eta)^2}} \arctan\left[\frac{1+\frac{1}{\sqrt{3}}(1-\eta)}{\sqrt{1-\frac{1}{\sqrt{3}}(1-\eta)^2}}\tan\left(\frac{\theta}{2}\right)\right]\right\} + 4\eta - 4\eta_{critical-y} \tag{23}$$

This expression is correct for evaluating the effec–tiveness of ligaments from η = 100% up to a critical efficiency coefficient of 50%, i.e. $\eta_{critical\text{-}x}$ = 50%.

For the *z*-direction it follows that:

$$\frac{E_z^*}{E_z} = h(\eta), \quad h(\eta) = 1 - \frac{\pi}{2\sqrt{3}}(1-\eta)^2 \tag{24}$$

By knowing the modulus of elasticity*E*and Poisson's ratio *v* in all three directions, the shear modulus can be obtainedusing a standard formula $G = \frac{E}{2(1+\nu)}$

The nine necessary material constants for an ortho–tropic plate were obtained.

3.6. Stress multipliers

The matrix establishing the dependence of equivalent strains and equivalent stresses is:

$$\begin{pmatrix} \varepsilon_{xx}^* \\ \varepsilon_{yy}^* \\ \varepsilon_{zz}^* \\ \varepsilon_{yz}^* \\ \varepsilon_{zx}^* \\ \varepsilon_{xy}^* \end{pmatrix} = \begin{pmatrix} \frac{1}{E_x^*} & \frac{-v_{yx}^*}{E_y^*} & \frac{-v_{zx}^*}{E_z^*} & 0 & 0 & 0 \\ \frac{-v_{yx}^*}{E_y^*} & \frac{1}{E_y^*} & \frac{-v_{zy}^*}{E_z^*} & 0 & 0 & 0 \\ \frac{-v_{zx}^*}{E_z^*} & \frac{-v_{zy}^*}{E_z^*} & \frac{1}{E_z^*} & 0 & 0 & 0 \\ 0 & 0 & 0 & \frac{1}{2G_{yz}^*} & 0 & 0 \\ 0 & 0 & 0 & 0 & \frac{1}{2G_{zx}^*} & 0 \\ 0 & 0 & 0 & 0 & 0 & \frac{1}{2G_{xy}^*} \end{pmatrix} \begin{pmatrix} \sigma_{xx}^* \\ \sigma_{yy}^* \\ \sigma_{zz}^* \\ \sigma_{yz}^* \\ \sigma_{zx}^* \\ \sigma_{xy}^* \end{pmatrix} \tag{25}$$

A link for isotropic material:

$$\begin{pmatrix} \varepsilon_{xx} \\ \varepsilon_{yy} \\ \varepsilon_{zz} \\ \varepsilon_{yz} \\ \varepsilon_{zx} \\ \varepsilon_{xy} \end{pmatrix} = \begin{pmatrix} \frac{1}{E} & \frac{-\upsilon}{E} & \frac{-\upsilon}{E} & 0 & 0 & 0 \\ \frac{-\upsilon}{E} & \frac{1}{E} & \frac{-\upsilon}{E} & 0 & 0 & 0 \\ \frac{-\upsilon}{E} & \frac{-\upsilon}{E} & \frac{1}{E} & 0 & 0 & 0 \\ 0 & 0 & 0 & \frac{1}{2G} & 0 & 0 \\ 0 & 0 & 0 & 0 & \frac{1}{2G} & 0 \\ 0 & 0 & 0 & 0 & 0 & \frac{1}{2G} \end{pmatrix} \begin{pmatrix} \sigma_{xx} \\ \sigma_{yy} \\ \sigma_{zz} \\ \sigma_{yz} \\ \sigma_{zx} \\ \sigma_{xy} \end{pmatrix} \tag{26}$$

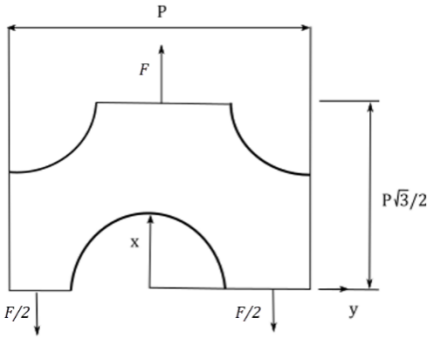

Figure 8. The smallest triangular repeating motif

The relationship between stress and strain in the form of the inverse elasticity operator as an action of the stiffness operator is given by the matrix relation:

$$\begin{pmatrix}\sigma_{xx}^*\\ \sigma_{yy}^*\\ \sigma_{zz}^*\\ \sigma_{yz}^*\\ \sigma_{zx}^*\\ \sigma_{xy}^*\end{pmatrix}=\begin{pmatrix}\frac{1-\upsilon_{yz}^*\upsilon_{zy}^*}{E_y^*E_z^*\Delta} & \frac{\upsilon_{yx}^*-\upsilon_{zx}^*\upsilon_{yz}^*}{E_y^*E_z^*\Delta} & \frac{\upsilon_{zx}^*-\upsilon_{yx}^*\upsilon_{zy}^*}{E_y^*E_z^*\Delta} & 0 & 0 & 0\\ \frac{\upsilon_{yx}^*-\upsilon_{zx}^*\upsilon_{yz}^*}{E_y^*E_z^*\Delta} & \frac{1-\upsilon_{zx}^*\upsilon_{xz}^*}{E_z^*E_x^*\Delta} & \frac{\upsilon_{zy}^*-\upsilon_{zx}^*\upsilon_{xy}^*}{E_z^*E_x^*\Delta} & 0 & 0 & 0\\ \frac{\upsilon_{zx}^*-\upsilon_{yx}^*\upsilon_{zy}^*}{E_y^*E_z^*\Delta} & \frac{\upsilon_{zy}^*-\upsilon_{zx}^*\upsilon_{xy}^*}{E_z^*E_x^*\Delta} & \frac{1-\upsilon_{xy}^*\upsilon_{yx}^*}{E_x^*E_y^*\Delta} & 0 & 0 & 0\\ 0 & 0 & 0 & 2G_{yz}^* & 0 & 0\\ 0 & 0 & 0 & 0 & 2G_{zx}^* & 0\\ 0 & 0 & 0 & 0 & 0 & 2G_{xy}^*\end{pmatrix}\begin{pmatrix}\varepsilon_{xx}^*\\ \varepsilon_{yy}^*\\ \varepsilon_{zz}^*\\ \varepsilon_{yz}^*\\ \varepsilon_{zx}^*\\ \varepsilon_{xy}^*\end{pmatrix} \tag{27}$$

where it follows according to Cepkauskas [22]:

$$\Delta=\frac{1-\upsilon_{xy}^*\upsilon_{yx}^*-\upsilon_{yz}^*\upsilon_{zy}^*-\upsilon_{zx}^*\upsilon_{xz}^*-2\upsilon_{xy}^*\upsilon_{yz}^*\upsilon_{zx}^*}{E_x^*E_y^*E_z^*} \tag{28}$$

Equations (25), (26), (27) can now be written in matrix notation as:

$$\begin{aligned}\varepsilon^* &= C^*\sigma^*\\ \varepsilon &= C\sigma\\ \sigma^* &= C^{*-1}\varepsilon^*\end{aligned} \tag{29}$$

Throughout this analysis, it was assumed that $\varepsilon = \varepsilon^*$ so $C^*\sigma^*$ we equate with $C\sigma$ and solve for σ:

$$\sigma = C^*C^{-1}\sigma^* = M\sigma^* \tag{30}$$

M is a 6 X 6 matrix of stress multipliers to convert average fictitious stress to average real stresses in the plate.

3.7. Application to a perforated thin-walled cylinder

The analytical model of a smooth cylinder in cylindrical coordinates neglects parameters along the radial component.In this way, the 6 x 6 matrix operators are reduced to 3 x 3 matrix operatorsand the *E*of the smooth cylinder is isotropic as well as that of the flat plate.

Stresses $\sigma\sigma_{xx}(x,\phi)$, $\sigma\sigma_{yy}(x,\phi)$, $\sigma\sigma_{xy}(x,\phi)$ are now stresses in the cylindrical coordinate system $\sigma_z(z,\phi)$, $\sigma_\phi(z,\phi)$, $\tau_{z,\phi}(z,\phi)$.

It follows:

$$\varepsilon^* = \begin{pmatrix}\varepsilon_z^*\\ \varepsilon_\phi^*\\ \varepsilon_{z\phi}^*\end{pmatrix} \tag{31}$$

$$\varepsilon^* = \begin{pmatrix}\frac{1}{E_z^*} & \frac{-\upsilon_{z\phi}^*}{E_\phi^*} & 0\\ \frac{-\upsilon_{z\phi}^*}{E_\phi^*} & \frac{1}{E_\phi^*} & 0\\ 0 & 0 & \frac{1}{2G_{z\phi}^*}\end{pmatrix}\begin{pmatrix}\sigma_z^*\\ \sigma_\phi^*\\ \tau_{z\phi}^*\end{pmatrix} \tag{32}$$

The matrix M is:

$$M=\begin{pmatrix}-\frac{E}{E_z^*(\upsilon^2-1)}+\frac{\upsilon_{z\phi}^*\upsilon E}{E_\phi^*(\upsilon^2-1)} & -\frac{\upsilon E}{E_z^*(\upsilon^2-1)}+\frac{\upsilon_{z\phi}^*E}{E_\phi^*(\upsilon^2-1)} & 0\\ \frac{\upsilon_{z\phi}^*E}{E_\phi^*(\upsilon^2-1)}-\frac{\upsilon E}{E_\phi^*(\upsilon^2-1)} & \frac{\upsilon_{z\phi}^*\upsilon E}{E_\phi^{\,*}(\upsilon^2-1)}-\frac{E}{E_\phi^*(\upsilon^2-1)} & 0\\ 0 & 0 & \frac{G}{G_{z\phi}^*}\end{pmatrix} \tag{33}$$

At the end it follows:

$$\sigma=\begin{pmatrix}\sigma_z\\ \sigma_\phi\\ \tau_{z\phi}\end{pmatrix}=\begin{pmatrix}-\frac{E}{E_z^*(\upsilon^2-1)}+\frac{\upsilon_{z\phi}^*\upsilon E}{E_\phi^*(\upsilon^2-1)} & -\frac{\upsilon E}{E_z^*(\upsilon^2-1)}+\frac{\upsilon_{z\phi}^*E}{E_\phi^*(\upsilon^2-1)} & 0\\ \frac{\upsilon_{z\phi}^*E}{E_\phi^*(\upsilon^2-1)}-\frac{\upsilon E}{E_\phi^*(\upsilon^2-1)} & \frac{\upsilon_{z\phi}^*\upsilon E}{E_\phi^{\,*}(\upsilon^2-1)}-\frac{E}{E_z^*(\upsilon^2-1)} & 0\\ 0 & 0 & \frac{G}{G_{z\phi}^*}\end{pmatrix}\begin{pmatrix}\sigma_z^*\\ \sigma_\phi^*\\ \tau_{z\phi}^*\end{pmatrix} \tag{34}$$

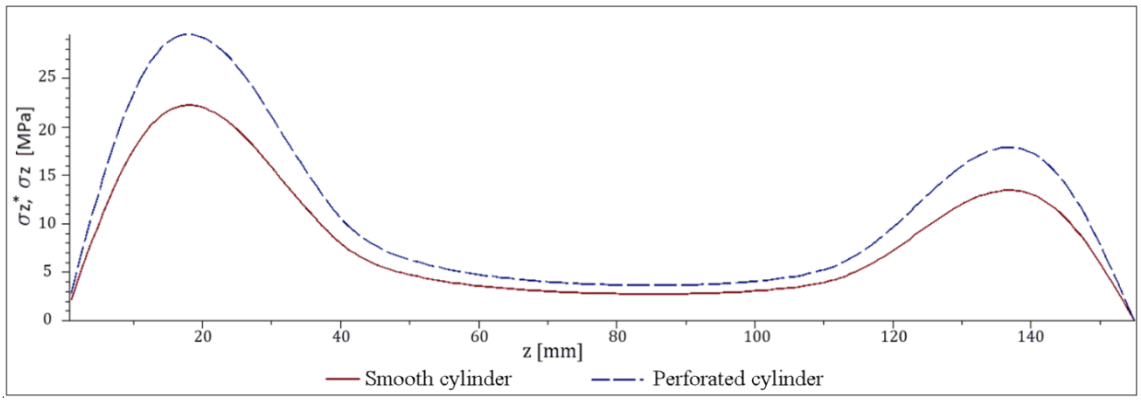

Figure 9. Comparative $\sigma_z(z,\phi)$ along the *z*-axis for a smooth and perforated cylinder

The equivalent plate is represented by a smooth cy–linder, and the values of its modulus of elasticity and Poisson's coefficient are geometrically redefined.

The stresses $\sigma_z^*(z,\phi)$, $\sigma_\phi^*(z,\phi)$ $\sigma_{z\phi}^*(z,\phi)$ are va–lues obtained by calculation for a smooth cylinder, while the stresses $\sigma_z(z,\phi)$, $\sigma_\phi(z,\phi)$ $\sigma_{z\phi}(z,\phi)$ are for a perforated cylinder, as in expression (34).

Example:

As applied in this paper, the criterion for choosing the parameters of the temperature distribution function $T(z,\phi)$ that figures in the mathematical model is the greatest possible similarity with the real temperature field. The results of the combustion simulation in the numerical CFD simulation of the gas burner with perforation were used as the temperature field [20]. With the help of this CFD simulation, the temperature field $T(z,\phi)$ was obtained as a load on the outer sheath,in this way yielding temperature distribution on the outer sheath for a burner with a length of 154 mm and a diameter of 80 mm.

After calculating the stress, this result was used to compare the stress on the plate with the redefined stresses on the cylinder with a triangular arrangement of holes with a diameter 0,6 *mm.*

Figure 9 shows both $\sigma_z^*(z,\phi)$ and $\sigma_z(z,\phi)$ along the *z*-axis for a smooth and perforated cylinder. Stresses for a smooth and perforated cylinder for temperature distribution parameters according to the expression (15)of the function $T(z,\phi$ for values T = 335K, l = 88 mm, b = 55 mm, $\theta = \pi/4$.

4. CONCLUSION

In the available literature, it has not been noticed that someone has created a comprehensive unique model that would unify all the influence segments and in such a way optimize the geometry of the cylindrical burner.

The presented thermomechanical model expanded and unified the mathematical stress model for a thin-walled smooth cylinder with the mathematical stress model for a perforated thin-walled cylinder exposed to uneven thermal loads.This unique model opens up op–portunities for analysis and optimization of different forms of perforations in thin-walled cylinders exposed to uneven thermal stresses.

In the future research, additional CFD numerical simulations should be made and mathematical results compared for different forms of perforations of thin-walled cylinders.

REFERENCES

[1] Erne, S., Scheger, G., Wiedemair, W.: Numerical and Experimental Investigation of Surface-Stabilized Combustion in a Gas-Fired Condensing Boiler, Elsevier, Results in Engineering, Vol. 17, 100738, 2023.

[2] Schiro, F.,Stoppato, A. and Benato, A.: Gas fired boilers: Perspective for near future fuel composition and impact on burner design process, E3S Web of Conferences 22, 00154, ASEE17, Vol. 22, 2017.

[3] Lamioni, R., Bronzoni, C., Folli, M., Tognotti, L. and Galletti, C.: Effect of slit pattern on the structure of premixed flames issuing from perforated burners in domestic condensing boilers, Combustion Theory and Modelling, Volume 27-Issue 2, pp. 218-243, 2023.

[4] Prochaska, B., Radić, N. and Gvero, P.: Numerical research of thermal stress in a gas burner with a cylindrical mantle in relation to its construction, Journal of Physics: Conference Series, Vol. 1426, 2020.

[5] Moghaddam, M. H. S.,Moghaddam. M. S. and Khorramdel, M.: Numerical study of geometric parameters effecting temperature and thermal efficiency in a premix multi-hole flat flame burner, Elsevier Ltd. Energy 125, pp. 654-662, 2017.

[6] Zhao, D.-F.,Liu, F.-G., You, X.-Y.,Zhang, R.,Zhang, B.-L.,He, G.-L.: Optimization of a premixed cylindrical burner for low pollutant emission, Elsevier Ltd. Energy Conversion and Management Vol. 99, pp.151–160, 2015.

[7] Liu, F.-G.,You, X.-Y.,Wang, Q.,Zhang, R.: On optimal design and experimental validation of household appliance burner of low pollutant emission, Elsevier Ltd. Energy Conversion and Management Vol. 76, Pages 837-845, 2013.

[8] Veetil, J. E., Aravind, B.,Mohammad, A.,Kumar, S.,Velamati, R. K., Effect of hole pattern on the

structure of small-scale perorated plate burner flames, Elsevier Ltd. Fuel Vol. 216, pp. 722–733, 2018.

[9] Gvero, P., Lekic, S., Vojinović, Đ. and Prochaska, B.: Design and Modelling Aspects in Premixed Gas Burners Development, *SDEWES 2016, Digital Proceedings paper 0383*, Lisbon, 2016. pp. 0383-1 – 0383-18.

[10] Evci, C.,Gülgeç, M.: Functionally graded hollow cylinder under pressure and thermal loading: Effect of material parameters on stress and temperature distributions, Elsevier Ltd. International Journal of Engineering Science Vol. 123, pp. 92–108, 2018.

[11] Elgezzar, M.,Rashad, A.,Hassan, M. S.,Elnady, T.: CFD Analysis and Geometrical Parameter Investigation for The Design of A High-Efficiency Supersonic Ejector, FME Transactions, Vol. 52, pp. 1-11, 2024.

[12] Ovais A. A., Khobragade, N.W. Khalsa, L.H.: Thermal Stress Analysis of a thin Hollow Cylinder: Transient Problem, International Journal of Engineering and Innovative Technology, Vol. 6, pp.42-47, 2016.

[13] Milošević-Mitić, V., Petrović, A., Anđelić, N.,Jovanović, M.: The Influence of Temperature Gradient on Thin Plates Bending, FME Transactions, Vol. 52, pp. 128-135, 2024.

[14] Aziz, A.,TorabiM.: Thermal Stresses in a Hollow Cylinder with Cinvective Boundary Conditions on the Inside and Outside Surfaces, Journal of Thermal Stresses, Vol.36 pp. 1096-1111, 2013.

[15] Jiawei, X. and Huang, Y.: Estimate of Temperature Gradients of Thin-Walled Structures under Thermomechanical Fatigue Loading, Jurnal of American Institute of Aeronautics and Astronautics, Inc., Vol. 60, No.9, pp. 5489-5499, September 2022.

[16] Dehghani, M.,Fotuhi, A. R., Shafiei, A. R.: Thermal Stress Analysis in a Finite Perforated Plane, Springer, Iranian Journal of Science and Technology, Transactions of Mechanical Engeering, Vol. 43, 705–721, 2019.

[17] Tooth, A. S.,Panayotti, A.,Owen, R.:The Thermal Behaviour of Thin Cylindrical Shells-II. Elastic Thermal Stress Analysis, Elsevier Ltd., International Journals of Mechanical Science, Vol. 31, Issue 9, pp. 707-716, 1989.

[18] Sanders, J. Lyell: An Improved First-Approximation Theory for Thin Shells, National Aeronautics and Space Administration, Technical Report R-24, Washington, 1959.

[19] WILSON, J. D.: Thermal Stresses in Thin Cylindrical Shells, SMiRT 2 - 2nd Int. Conf. Structural Mechanics in Reactor Technology, Berlin, Germany, 1973.

[20] Prochaska, B., *Optimization of high perforation gas burners with the aim to reduce thermal stresses*, in PhD thesis, University of East Sarajevo, Faculty of Mechanical Engineering, 2022.

[21] Tooth, G. Duthieand A. S., Local loads on cylindrical vessels. A Fourier series solution. In Behaviour of Thin Walled Structures, Elsevier Applied Science (Edited by RHODES and SPENCE), pp. 235-272, 1984.

[22] Cepkauskas, J. Y. M.M.: Equivalent Properties for Perforated Plates - An Analytical Approach, *18th International Conference on Structural Mechanics in Reactor Technology SMiRT 18-F06-1*, 2005.

[23] Prochaska, B., Radić, N., Živković, P., Tomić, M., Škundrić, J.: Perforated Household Burner Stress Modeling, Innovative Mechanical Engineering, Vol. 2, No 1, pp. 1 – 9, 2023.

NOMENCLATURE

R, t, L	Mean radius, cylinder thickness, cylinder length
r, ϕ, z	Cylindrical coordinates
e_z, e_ϕ, $e_{z\phi}$	Total deformations
σ_z, σ_ϕ, $\tau_{z\phi}$	Normal and tangential stresses
σ_z^*, σ_ϕ^*, $\tau_{z\phi}^*$	Equivalent normal and tangential stresses
E	Modulus of elasticity
E^*	Equivalent modulus of elasticity
ν	Poisson's ratio
ν^*	Equivalent Poisson's ratio
α	Coefficient of thermal expansion
T	Temperature
ε_z, ε_ϕ, $\varepsilon_{z\phi}$	Deformations in the middle of the shell
k_z, k_ϕ, $k_{z\phi}$	Deformations due to curvature changes
$u(z,\phi)$, $v(z,\phi)$, $w(z,\phi)$	Displacements in a cylindrical coordinate system
R	The radius of the central surface of the shell
N_z, N_ϕ, $N_{z\phi}$	Resultants of forces
M_z, M_ϕ, $M_{z\phi}$	Bending moments

P_x, P_ϕ, P_r	Components of external forces
T_M	Temperature on the outer surface of the cylinder
T_D	Temperature difference of the inner and outer surface
t	Shell thickness
N_T	Thermal force
M_T	Thermal bending moment
K	Expansion rigidity
D	Bending rigidity
G	Shear modulus
n,m	Harmonic members in angular and axial directions
λ_m	$= \frac{m\ \pi\ R}{L}$
d,δ	$d = \frac{\partial}{\partial(z/R)} = R\frac{\partial}{\partial z}, \quad \delta = \frac{\partial}{\partial \phi}$
P	Perforation step
h	Connection between weakening surfaces, ligament
η	Connection efficiency, solid and perforated plates

МЕХАНИЧКО МОДЕЛИРАЊЕ ТЕРМОМЕХАНИЧКИХ ПРОЦЕСА

Б. Прохаска, Н. Радић, С. Булатовић

Анализиран је проблем напрезања у перфорираним танкозидним цилиндрима усљед механичког и топлотног оптерећења за случајеве гдје оптерећење система варира и по ободу цилиндра и аксијално. Полазећи од рјешења и разматрања за пуни танкозидни цилиндар, овдје је проширен концепт и посматрана је расподјела деформација насталих топлотним оптерећењем на цилиндар и насталих напона у структури танкозидног перфорираног цилиндра за конкретан облик перфорације.

Уређај на чијем се усавршавању континуирано ради је предмијешаникондензациони котао за кућне системе грijања. Цилиндрични перфорирани горио–ник је један од главних елемената овог уређаја. Од распореда, облика и димензија перфорације у многоме зависи квалитет сагоријевања, а самим тим и топлотног оптерећења на вањском плашту овог горионика.

У овом раду је приказано механичко моделирање термомеханичких процеса цилиндричног гасног горионика са предмијешањем за троугаони распоред или такозвани шаховски облик перфорације.